1    **CD161 mediates prenatal immune suppression of IFNγ-producing PLZF+ T cells**

2    Joanna Halkias[*1], Elze Rackaityte[2], Dvir Aran[3], Ventura F. Mendoza[4], Walter L.

3    Eckalbar[5], and Trevor Burt[1,4]

4

5    [1]Division of Neonatology, Department of Pediatrics, University of California, San Francisco, CA,

6    94131, USA.

7    [2]Biomedical Sciences Program, University of California, San Francisco, CA, 94143, USA.

8    [3]Institute for Computational Health Sciences, University of California, San Francisco, California,

9    94158, USA

10   [4]Eli and Edythe Broad Center of Regeneration Medicine and Stem Cell Research, University of

11   California, San Francisco, San Francisco, CA, 94143, USA

12   [5]Department of Medicine, University of California San Francisco, San Francisco, CA, 94158,

13   USA.

14

15   **SUMMARY**

16

17       While the fetal immune system defaults to a program of tolerance, there is concurrent

18   need for protective immunity to meet the antigenic challenges after birth. Activation of fetal T cells

19   is associated with fetal inflammation and the termination of pregnancy, yet which fetal T cells

20   contribute to this process is poorly understood. Here we show a transcriptionally distinct

21   population of pro-inflammatory T cells that predominates in the human fetal intestine. Activation of

22   PLZF+ T cells results in rapid production of Th1 cytokines and is inhibited upon ligation of surface

23   CD161. This mechanism of fetal immune suppression may inform how immune dysregulation

24   could result in fetal and neonatal inflammatory pathologies such as preterm birth. Our data

25   support that human development of protective adaptive immunity originates *in utero* within the

26   specialized microenvironment of the fetal intestine.

27

28   **INTRODUCTION**

29

30    The developing human immune system is uniquely adapted for fetal survival within the semi-

31    allogeneic environment *in utero* as well as for neonatal protection after contact with the many

32    antigenic challenges encountered after birth. Unlike mice, which lack peripheral T cells *in utero,*

33    human T cells begin to populate peripheral organs (including mucosal sites) by 11-14 weeks of

34    gestation [1,2]. While naïve fetal T cells preferentially generate induced regulatory T cells upon

35    antigen encounter in the periphery [3], there is evidence of protective fetal adaptive immunity in

36    response to pathogens and vaccines [4-6]. However, activated T cells are associated with the fetal

37    inflammatory response and contribute to the comorbidities associated with preterm birth [7-11]. The

38    concurrent development of fetal tolerogenic and protective T cell programs indicate that human

39    immune development may be more nuanced than previously appreciated.

40

41    The presence of functional memory T cells in the fetus and infant [12-15] indicate that adaptive

42    immune memory originates *in utero*. However, the spatial compartmentalization of human T cell

43    differentiation and function suggests that the effector capacity of the fetal immune response

44    cannot be inferred from blood [13,16,17]. The existence of organized intestinal lymphoid structures as

45    early as the second trimester of gestation [18], along with the environmental, maternal, and self-

46    antigens within swallowed amniotic fluid, points to an instructive role for the intestinal mucosa in

47    the development of fetal adaptive immunity.

48

49    In this study, we performed a detailed examination of fetal lymphoid and mucosal TCR$\alpha\beta$ CD4$^+$ T

50    cells. We identified a polyclonal population of IFN$\gamma$-producing T cells characterized by expression

51    of the transcription factor Promyelocytic Leukemia Zinc Finger (PLZF) and the C-type lectin

52    CD161. These Va7.2$^-$ PLZF$^+$ CD161$^+$ TCR$\alpha\beta^+$ CD4$^+$ T cells preferentially accumulate in the

53    lamina propria (LP) of the small intestine and possess a resident memory phenotype inferred

54    from expression of CD69 and CD103 [19]. We demonstrate that Va7.2$^-$ PLZF$^+$ CD161$^+$ TCR$\alpha\beta^+$

55    CD4$^+$ T cells, herein referred to as polyclonal intestinal (pi) PLZF$^+$ CD161$^+$ T cells, are

56    transcriptionally distinct and possess a type 1 T helper (Th1) functional signature, which identifies

57    them as a major effector population in the fetal intestine. We also show that the ability of these

58    fetal T cells to produce IFN$\gamma$ is positively associated with advancing gestation. We found that

59    Lectin-like transcript 1 (LLT1), the ligand for CD161, was uniquely expressed by resident

60    macrophages of the intestine, and that ligation of CD161 inhibited the TCR-mediated activation of

61    pi-PLZF+ CD161+ T cells. We propose a model in which functional maturation of pi-PLZF+

62    CD161+ T cells occurs under steady state in a spatially segregated manner in the lamina propria

63    of the intestine, where CD161 mediates immune suppression and allows for induction of immunity

64    uncoupled from inflammation. The ability  of pi-PLZF+ CD161+ T cells to respond to both TCR-

65    and cytokine-mediated signaling suggests a potential for these cells to contribute to the multitude

66    of inflammatory pathologies associated with premature birth. Our identification of the suppressive

67    role of CD161 points to a putative therapeutic target to control the fetal inflammatory response for

68    which there is currently no effective therapy.

69

70

71    **RESULTS**

72

73    **Memory PLZF+ CD4+ T cells are highly enriched in the fetal small intestine**

74    The human fetal thymus produces a subset of CD4+ T cells which express the transcription factor

75    PLZF and are distinct from iNKT cells and MAIT cells1 [20]. To explore whether PLZF+ T cells

76    contribute to the development of protective immunity *in utero*, we examined their distribution in

77    mucosal and lymphoid tissue. PLZF expression was abundant among lamina propria (LP) CD4+ T

78    cells of the fetal small intestine (Fig. 1a). As many human innate cells express PLZF (cite), we

79    restricted our analysis to TCR$\beta$+ Va7.2- CD4+ T cells, which excluded innate lymphoid cells, MAIT

80    cells, and $\gamma\delta$ T cells (Supplementary Fig. 1). PLZF+ T cells accounted for ~30% of all intestinal

81    V$\alpha$7.2- TCR$\alpha\beta$+ CD4+ T cells, whereas they averaged <10% of CD4+ T cells across all other

82    lymphoid and non-lymphoid sites with the exception of the appendix (Fig. 1b, c). Adult human

83    PLZF+ T cells often co-express the C-type lectin CD161, which identifies T cells with innate

84    characteristics [21]. The majority of intestinal PLZF+ T cells and ~ half of those in the appendix were

85    CD161^{+}, whereas less than half of PLZF^{+} T cells across other sites expressed CD161 (Fig. 1b, d).

86    Consistent with the reported decline in thymic production of PLZF^{+} CD4^{+} T cells with advancing

87    gestation [20,22], PLZF^{+} CD4^{+} T cells are essentially undetectable in term cord blood (CB) and adult

88    peripheral blood (aPB), and we used aPB samples as internal controls between experiments

89    (Extended Fig. 1a-b).

90

91    Previous studies have identified memory T cells in fetal and neonatal small intestine [12,13,23,24],

92    which led us to examine the maturation state of intestinal T cells on the basis of CD45RA and

93    CCR7 expression. The majority of intestinal PLZF^{+} CD4^{+} T cells had a CD45RA^{-} CCR7^{-} effector

94    memory (T$_{EM}$) phenotype (85% of PLZF^{+}CD161^{+} and 60% of PLZF^{+} CD161^{-}) and contained

95    significantly less naïve cells than PLZF^{-} T cells (Extended Fig. 1c & Fig. 1e). This held true across

96    multiple tissues, where PLZF^{+} CD161^{+} T cells were significantly more likely than PLZF^{-} T cells to

97    possess a T$_{EM}$ phenotype in the MLN, and trended towards more T$_{EM}$ in the appendix and spleen

98    (Extended Fig. 1d). In contrast, PLZF^{-} CD4^{+} T cells had a more even distribution of naïve, central

99    memory (T$_{CM}$) and T$_{EM}$ cells, similar to that reported for infant and pediatric intestine [12,13]. Most

100   intestinal PLZF^{+} T cells were CD69^{+}, and ~20% also expressed CD103 consistent with a resident

101   memory (T$_{RM}$) phenotype (Extended Figure 2e) [13,16,25]. Overall, a T$_{RM}$ phenotype was most

102   frequent among intestinal PLZF^{+}CD161^{+} T cells (Fig. 1f).

103

104   **PLZF^{+} CD161^{+} CD4^{+} T cells are a transcriptionally distinct population of mucosal T cells**

105   To investigate whether intestinal PLZF^{+} T cells represent a distinct population of fetal T cells, we

106   determined their global gene expression profile and examined their relationship to innate, semi-

107   invariant Va7.2^{+} T cells and to conventional PLZF^{-} CD4^{+} memory T cells (Extended Fig. 2a). We

108   sorted semi-invariant innate T cells on the basis of TCR$\beta$[+] V$\alpha$7.2^{+} CD161^{+} cells [26,27], of which the

109   majority (>75%) were also IL18R^{+} (Extended Fig. 2b).  Although not exclusive for mucosal-

110   associated invariant T (MAIT) cells, this subset is enriched for MAIT cells [28]. We identified

111   additional surface markers that allowed us to separate PLZF^{+} from PLZF^{-} memory CD4^{+} T cells

112   (Extended Fig. 2b, c, Supplementary Table 1). The expression of *ZBTB16*, *IL18R*, *PDCD1*, and

113    *KLRB1* (the respective genes for PLZF, IL18R, PD1 and CD161) mirrored their protein

114    expression and validated our sorted T cell populations and our gene expression analysis

115    (Extended Fig. 2d). Intestinal PLZF⁺ T cells formed a spatially separate group from either semi-

116    invariant innate T cells or PLZF⁻ memory T cells, reflecting a divergent transcriptional state by

117    principal component analysis (PCA) (Fig. 2a). PLZF⁺ T cells were highly distinct by principal

118    component (PC) 1 (23% of variance) and segregated between PLZF⁻ T cells and semi-invariant

119    innate T cells along PC2 (19.9% of variance), suggesting shared attributes with these

120    populations. Twice as many genes were enriched in PLZF⁺ relative to PLZF⁻ memory T cells

121    (499) as compared to semi-invariant innate T cells (278) (>2-fold, FDR<0.05)(Fig. 2b).

122

123    We first focused on the genes that differentiated PLZF⁺ T cells from conventional PLZF⁻ T cells

124    and utilized the Human Protein Cell Atlas as a reference to identify genes that cluster together by

125    cell type using correlation analysis [29]. This identified 6 clusters, of which clusters 2 and 4 were

126    comprised predominantly of myeloid-associated genes (Fig. 2c, Extended Fig. 3a). Among the

127    myeloid genes in cluster 4 were those associated with immune regulation (GAB2, NLRP3,

128    TGFB1, and C3AR1), while myeloid-enriched genes in cluster 2 were involved in lipid metabolism

129    (PPARG, PLIN2, and NFIL3) (Extended Fig 3b). Cluster 6 was enriched for stem cells and

130    contained genes involved in the cell cycle from which we inferred that PLZF⁺ T cells were likely

131    proliferating *in vivo* (Extended Fig. 3b, Supplementary Figure 2). Cluster 1 was enriched for

132    genes associated with immune activation and overlapped with effector memory T cells, NK cells,

133    and $\gamma\delta$ T cells suggestive of effector properties including Th1-like and cytotoxic functions

134    (Extended Fig. 3b, Supplementary Figure 2). This correlation analysis allowed us to extrapolate

135    function based on expression overlap with other cell types, and revealed an atypical composition

136    of myeloid-, lymphoid-, and stem cell-associated genes in PLZF⁺ T cells.

137    A striking difference in the genes differentially expressed between PLZF⁺ T cells and semi-

138    invariant innate T cells was the diversity of TCR usage. A number of TRAV regions were enriched

139    in PLZF⁺ T cells, while semi-invariant innate T cells displayed preferential expression of TRBV9,

140    TRBV7-9, and TRBV6-4 which have been associated with MAIT cells [30,31] (Extended Fig. 3d).

141  The polyclonal nature of PLZF⁺ T cells was supported by variable Vβ use among both PLZF⁺ and

142  PLZF⁻ T cells and was comparable to that reported in fetal blood [32] with no single chain

143  accounting for >10% of TCR Vβ families (Extended Fig. 3e).

144

145  We identified a core signature of 111 genes that were enriched, and 137 genes that were

146  depleted in PLZF⁺ T cells compared to both PLZF⁻ T cells and semi-invariant innate T cells

147  (>2FC; FDR<0.05) (Fig. 2d, Extended Fig. 3f).  PLZF⁺ T cells demonstrated distinct gene

148  expression profiles enriched in immune activation pathways, as well as genes involved in the

149  regulation of the immune response (Fig. 2d). Specifically, the core signature of PLZF⁺ T cells

150  contained transcripts involved in T cell activation (IL2, CD40LG, IL18R1, IL2RB, MAP3K8,

151  PIK3R1), as well as T cell regulation (DUSP4, DUSP5, DUSP6, LRIG1, and DTX1).  Among the

152  genes specifically depleted in PLZF⁺ T cells were those required for lymph node homing and

153  tissue egress (*SELL, CCR7, S1PR1, KLF2*) [19], supporting the characterization of these cells as

154  human T_RM cells. We therefore define a transcriptionally unique subset of polyclonal intestinal

155  PLZF⁺ CD4 T cells, which share gene expression profiles with innate immune cells suggestive of

156  a rapid effector phenotype. However, the presence of numerous negative T cell regulators among

157  the gene signature of PLZF⁺ T cell points to cell-intrinsic mechanisms of regulation to promote

158  immune homeostasis *in utero*.


159  **PLZF⁺ CD4 T cells possess Th-1 effector function**

160  Lamina propria PLZF⁺ T cells produced large amounts of the Th1 cytokines TNFα and IFNγ upon

161  short-term polyclonal activation by Phorbol 12-myristate 13-acetate (PMA) and Ionomycin, and

162  expression of CD161 did not predict cytokine production among PLZF⁺ T cells (Fig. 3a, Extended

163  Fig. 4a, b). Among CD4 T cells, IFNγ was predominantly produced by PLZF⁺ cells, and intestinal

164  PLZF⁺ T cells produced more IFNγ than those of the mesenteric lymph node (MLN), spleen, or

165  thymus (Fig. 3b). While PLZF⁺ T cells also made more TNFα than their PLZF⁻ counterparts,

166  production of TNFα was less anatomically restricted and was already evident in >20% of thymic

167  PLZF⁺ T cells (Fig. 3c). Further, the capacity of PLZF⁺ T cells to produce IFNγ was directly

168  correlated with advancing gestation, but this association was not significant for TNF$\alpha$, nor

169  between either cytokine and PLZF$^-$ T cells (Fig. 3d, e & Extended Fig. 4c, d). Consistent with the

170  presence of *IL-2* in their core signature, intestinal PLZF$^+$ T cells produced more IL-2 than PLZF$^-$ T

171  cells, however production of IL-2 was equally abundant among MLN T cells (Extended Fig. 4e, g).

172  In contrast to Th1-asociated cytokines, IL-8 production was equivalent between PLZF$^+$ and PLZF$^-$

173  T cells and was lower in the intestine compared to the MLN (Extended Fig. 4f, h). Thus, in

174  addition to a core transcriptional signature, PLZF$^+$ T cells possess a Th1-type functional profile

175  and are an abundant source of IFN$\gamma$ in the fetal immune system.

176

177  **TCR-dependent and TCR-independent activation of PLZF$^+$ T cells**

178  We next assessed the signals required to trigger cytokine production in mucosal PLZF$^+$ T cells

179  and examined their response to stimulation through the T cell receptor (TCR). PLZF$^+$ T cells are

180  more responsive to short-term (12-16hrs) *in vitro* activation by anti-CD3/anti-CD28 monoclonal

181  antibodies (mAb) than PLZF$^-$ T cells, as indicated by higher production of both IFN$\gamma$ and TNF$\alpha$,

182  which more closely approximated their PMA/Ionomycin induced potential (Fig. 4a, b, Extended

183  Fig. 5a, b). The identification of both IL18R1 and IL18RAP within the core gene signature of

184  PLZF$^+$ T cells led us to additionally assess their response to TCR-independent activation.

185  Intestinal PLZF$^+$ T cells produced IFN$\gamma$ in response to the combination of IL-12 and IL-18, but not

186  to either cytokine alone (Fig. 4c). Stimulation with both IL-12 and IL-18 was able to approximate

187  the levels of IFN$\gamma$ production observed in response to PMA, yet failed to elicit production of TNF$\alpha$

188  (Extended Fig. 5c). Intestinal PLZF$^+$ T cells were more responsive to both TCR- and cytokine-

189  mediated activation than those in the thymus, which failed to produce significant levels of IFN$\gamma$

190  and suggested that maturation and acquisition of effector function occurred in the periphery

191  (Extended Fig. 5d). Therefore, we examined whether the memory phenotype of intestinal CD4 T

192  cells was indicative of different functional capacities. We found that the majority of the IFN$\gamma$

193  produced by intestinal CD4$^+$ T cells in response to either TCR signaling or cytokines alone

194  displayed an effector memory phenotype (PLZF$^+$ > PLZF$^-$ T cells) (Extended Fig. 5e), and that

195  PLZF$^+$ $T_{EM}$ cells produced significantly more IFN$\gamma$ than PLZF$^-$ $T_{EM}$ cells (Fig. 4d). Mucosal PLZF$^+$

196   T cells are therefore poised to generate a pro-inflammatory response to either TCR- and/or

197   cytokine-mediated activation, suggesting that their effector potential may be uniquely adapted for

198   mucosal immune surveillance.

199

200   **CD161 inhibits cytokine production in PLZF^{+} T cells**

201   The abundance of polyclonal intestinal (pi) PLZF^{+} T cells capable of responding to two different

202   methods of activation lead us to hypothesize that the behavior of these cells would be tightly

203   regulated.  The c-type lectin CD161 is expressed by the majority of intestinal pi-PLZF^{+} T cells and

204   has been ascribed conflicting roles in either the activation or inhibition of different human immune

205   cells [21,33,34]. LLT1, the natural ligand for CD161, was present on intestinal CD14^{+} antigen

206   presenting cells (APCs), whereas CD11c^{+} CD14^{-} dendritic cells (DCs) lacked expression of LLT1

207   (Extended Fig. 6a, Fig. 5a). Intestinal CD14^{+} APCs were CD68^{+}, CD163^{+}, CD209^{+}, expressed

208   intermediate levels of HLA-DR, and lacked expression of CD103, consistent with a tissue-resident

209   macrophage phenotype [35,36]  (Extended Fig. 6b). Macrophage LLT1 expression was not uniform

210   between samples, however LLT1 expression was consistently absent from intestinal DCs (Fig.

211   5b). The observed variability in LLT1 expression suggested that this ligand was acquired, which

212   prompted us to look for LLT1 expression across tissues with similar populations of APCs. A

213   similar CD14^{+} CD11c^{-} macrophage population in MLN and the appendix mirrored LLT1

214   expression of intestinal macrophages (Extended Fig. 6c, d),  and led us to explore the role of

215   CD161 in the regulation of fetal pi-PLZF^{+} T cells. We found that engagement of CD161 during

216   classical TCR activation resulted in potent inhibition of pi-PLZF^{+} T cells, reducing production of

217   both IFN$\gamma$ and TNF$\alpha$ (Fig. 5c, d). While two different clones of monoclonal antibodies to CD161

218   were equally effective at high dose (10$\mu$g/mL), clone HP3G10 consistently performed better at

219   lower doses (10$^{-1}$ to 10$^{-2}$$\mu$g/mL) (Fig. 5c, d). In contrast, cross-linking of CD161 did not inhibit

220   IFN$\gamma$ production by PLZF^{+} T cells in response to cytokine stimulation (Fig. 5e).

221

222   **DISCUSSION**

223

224    We have identified a polyclonal effector T cell population with a unique transcriptional profile and

225    Th1 functional properties which is abundant in the human fetal small intestine. The transcriptome

226    of pi-PLZF^{+} T cells displayed an unusual enrichment in myeloid-associated genes compared with

227    conventional CD4 T cells, which predicted the strong effector properties of these cells. In

228    conjunction with the ability to respond to cytokines independently of TCR activation, these gene

229    signatures highlight the innate-like qualities of pi-PLZF^{+} T cells, reminiscent of murine fetal CD5^{+}

230    B cells and TCRγδ T cells [37-39], as well as fetal MAIT cells and iNKT cells [24,27]. Unlike classic

231    innate-like T cells, MsFITs expressed a polyclonal TCR repertoire and accounted for up to half of

232    all CD4 T cells in the intestine. The dominant presence of Th1 pi-PLZF^{+} T cells with a distinct and

233    atypical transcriptome and shared attributes with innate immune cells suggests a role as a first

234    line of defense *in utero* and early life.

235

236    *In utero* development presents unique antigenic pressures to the fetus that might drive the

237    development and expansion of pi-PLZF^{+} T cells. Fetal T cells mount an antigen specific response

238    to semi-allogeneic maternal cells present within human fetal tissues, and fetal and neonatal T

239    cells show increased self-reactivity [3,40-42] . Further, recent reports of bacterial presence in human

240    meconium and amniotic fluid [43-45] challenge the paradigm that the fetus develops within a sterile

241    environment *in utero*. Intestinal MsFITs are functionally and anatomically positioned to encounter

242    antigen within swallowed amniotic fluid and could mount an immediate protective response. The

243    development of tissue resident T cell memory is closely coupled to anatomic location [19], and is

244    reflected in the increased ability of intestinal pi-PLZF^{+} T cells to produce Th1 cytokines, as well as

245    the preferential expression of the inhibitory receptor CD161. Multiple regulatory transcripts are

246    present in the core gene signature of pi-PLZF^{+} T cells, and we discovered CD161-mediated

247    inhibition pi-PLZF^{+} T cells as a previously unknown mechanism of immune suppression. The

248    presence of LLT1 on intestinal macrophages suggests they likely work in parallel with other

249    regulatory mechanisms to promote tolerance *in utero* [3,46-48]. We propose that as in the adult, there

250    is regional compartmentalization of the fetal effector response, and that the intestine is a

251    specialized niche which supports the development of protective immunity *in utero*.

252

253

254 **Material and Methods**

255 **Human tissues.** All human tissue obtained for analysis in this study was obtained with approval from and

256 under the guidelines of the UCSF Committee on Human Research. Human fetal tissue (small intestine,

257 appendix, mesenteric lymph node (MLN), spleen, liver, and thymus) was obtained under the auspices of

258 UCSF Committee on Human Research (CHR) approved protocols at 15-23 gestational weeks from San

259 Francisco General Hospital after informed consent from elective termination of pregnancy. Samples were

260 excluded in the case of (1) known maternal infection, (2) intrauterine fetal demise, and/or (3) known or

261 suspected chromosomal abnormality. Adult peripheral blood mononuclear cells (PB) derived from TRIMA

262 residues from TRIMA Apheresis collection kits were obtained from healthy donors after informed consent at

263 the Blood Centers of the Pacific. Umbilical cord blood (CB) from term infants was obtained in acid citrate

264 dextrose by sterile cordocentesis from the University of Texas MD Anderson Cancer Center in Houston,

265 Texas.

266

267 **Cell Isolation**. PBMCs from adult and cord blood were isolated by Ficoll-histopaque (Sigma Aldrich)

268 gradient centrifugation and cryopreserved in freezing medium composed of 90% FBS + 10% DMSO

269 (ATCC). Fetal organs were collected into cold RPMI with 10% FCS, 10 mM HEPES, penicillin, streptomycin,

270 0.1 mM 2-β-mercaptoethanol, 2 mM L-glutamine, and nonessential amino acids (cgRPMI medium),

271 transported on ice and processed within 2 hours of collection. The small intestine was dissected from the

272 mesentery, cut longitudinally, and meconium was removed with gentle scraping. The intestine was cut into

273 1cm sections and mucus was removed with three washes in 1mM DTT in PBS for 10 minutes. The epithelial

274 layer was removed with three washes in 1mM EDTA in PBS for 20 minutes. The intestine, MLN, liver, and

275 spleen were digested with freshly prepared 1mg/mL Collagenase IV (Life Technologies) and 10mg/mL

276 DNAse (Roche) in cgRPMI for 30 minutes, and dissociated cells were filtered through a 70um strainer. Cells

277 were separated in a 20%-40%-80% Percoll density gradient at 400 x g for 40 minutes.  T cells were

278 recovered at the 40-80% interface and APCs were recovered at the 20-40% interface, and all cells washed

279 twice in cgRPMI. All washes and incubations were performed in a shaking (200rpm) water bath at 37°C.

280 Thymocytes were isolated by gently pressing small pieces of thymus though a 70um strainer. Viability was

281 measured with Trypan Blue (Sigma Aldrich).

282   **Antibodies and flow cytometry.** Intestinal lamina propria (LP) T cells were isolated by negative selection

283   using the Easy Sep Human T cell isolation kit (STEMCELL Technologies).  Isolated cells were incubated in

284   2% FCS in PBS with 1mM EDTA (staining buffer) with human Fc block (STEMCELL Technologies) and

285   stained with fluorochrome-conjugated antibodies against surface markers. Intracellular protein detection was

286   performed on fixed, permeabilized cells using the Foxp3/Transcription Factor Staining Buffer set (Tonbo

287   Biosciences). Mouse anti-human mAbs used in this study include: TCRβ Percp-e710 (Clone IP26,

288   eBioscience Cat. No. 46-9986-42), Vα7.2 Biotin and BV605 (Clone 3C10, BioLegend Cat. No. 351720), CD4

289   APC H7 (Clone L200, BD Pharmingen Cat. No. 560837), CD8α FITC and PE (Clone B7-1, BD Pharmingen

290   Cat. No. 557226), CD45RA PE (Clone HI100, BD Pharmingen Cat. No. 555489), CCR7 BV421 (Clone

291   G043H7, BioLegend Cat. No. 353208), CD69 PE (Clone FN50, BioLegend Cat. No. 310906), CD103-FITC

292   (Clone Ber-ACT8, BD Pharmingen Cat. No. 550259), PLZF-APC (Clone 6318100, R&D Cat. No. IC2944A),

293   CD161-BV711 (Clone DX12, BD Biosciences Cat. No. 563865), IL18Rα-PE (Clone H44, BioLegend Cat. No.

294   313808), PD-1 BV605 (Clone EH12.2H7, BioLegend Cat. No. 329924), IFNγ-FITC (Clone 25723.11, BD

295   Biosciences Cat. No. 340449) TNFα-PE Cy7 (Clone MAB11, BD Pharmingen Cat. No. 557647), IL-2 (Clone

296   5344.11, BD Cat. No. 340448), IL-8 BV421 (Clone G265-8, BD Biosciences Cat. No. 563310), CD45 APC

297   (Clone HI30, Tonbo Cat. No. 20-0459), CD14 BV605 (Clone M5E2, BD Pharmingen Cat. No. 564054),

298   CD11c BB515 (Clone B-ly6, BD Pharmingen Cat. No. 564491), HLA-DR APC-R700 (Clone G46-6, BD Cat.

299   No. 565128), CD3 BV510 (Clone HIT3α, BD Cat. No. 564713), CD19 BV510 (Clone SJ25C1, BD Cat. No.

300   562947), CD56 BV510 (Clone NCAM16.2, BD Cat. No. 563041), CD68 PE Cy7 (Clone FA-11, BioLegend

301   Cat. No. 137016), CD163 BV711 (Clone GHI/61, BioLegend Cat. No. 333630), CD209 PerCP Cy 5.5 (Clone

302   DCN46, BD Pharmingen Cat. No. 558263), LLT1 PE (Clone 402659 R&D Cat. No. FAB3480P). TCRβ

303   repertoire profiling was performed by staining with the IOTest Beta Mark TCR V β Repertoire Kit (Beckman

304   Coulter). TCRβ repertoire profiling was performed by staining with the IOTest Beta Mark TCR V beta

305   Repertoire Kit (Beckman Coulter). All cells were stained with Aqua LIVE/DEAD Fixable Dead Cell Stain Kit

306   (Invitrogen) to exclude dead cells from analysis. All data were acquired with an LSR/Fortessa Dual SORP

307   flow cytometer (BD Biosciences) and analyzed with FlowJo V10.0.8 (TreeStar) software.

308

309   **Immunohistochemistry.** Intestinal sections were dissected and fixed in 4% paraformaldehyde for 10

310   minutes and subsequently passed through a sucrose gradient prior to embedding in OCT. Embedded

311   sections were then frozen on dry ice and stored at -80°C. 10um thin cryosections were obtained using a

312   cryostat and mounted on frosted charged slides. Histological work, imaging, and image processing was

313   performed by the Gladstone Institutes' Histology & Light Microscopy Core. Slides were fixed in acetone for 5

314   minutes at –20°C, rehydrated in PBS for 10 minutes, rinsed in 0.05% PBS-Tween, and permeabilized in

315   0.1% PBS-TritonX-100 for 15min at room temperature (RT). Slides were then blocked using 1% BSA, 0.1%

316   Fish skin gelatin, 0.5% TritonX-100, 0.05% Na-Azide in PBS for 2 hours and stained with purified anti-CD3

317   (clone Hit3a; BD Pharmingen, cat. # 555336) and anti-PLZF (clone NBPI-80894, Novus Biologicals, cat.

318   NBPI-80894) overnight at 4°C, followed by anti-CD4-eFluor 570 (N1UG0, Thermo-Fisher, cat. # 41-2444-82)

319   at RT for 3 hours. Slides were then incubated with secondary antibodies goat anti-mouse-DyLight 488

320   (Thermo Fisher, cat. # 35502) and goat anti-rabbit 633 (Thermo Fisher, cat. # A-21070) for 1 hour at RT,

321   stained with DAPI (Invitrogen) for 10 min at RT, and mounted with Fluormount-G (EMS). Images were

322   captured with a Zeiss Cell Observer Spinning Disk microscope (Carl Zeiss Microscopy, Thornwood, NY)

323   equipped with 405nm, 488nm, 561nm, 633nm lasers, Prime 95b sCMOS camera (Photometrics, Tucson,

324   AZ) and Zeiss Zen imaging software.

325

326   **T cell stimulation and CD161 inhibition.** For detection of basal cytokine potential, single cell suspensions

327   from various tissues were cultured directly *ex vivo* in a 96-well U-bottom plate in cgRPMI and stimulated with

328   50ng/ml phorbol myristate acetate (PMA) (Santa Cruz Biotechnology) and 5ug/ml ionomycin (Sigma-Aldrich)

329   in the presence of Brefeldin A (Sigma-Aldrich) for 3 hours at 37°C in 4% $O_2$ to mimic intra-uterine hypoxia.

330   Alternatively, T cells were cultured at 250k/well in 96-well plates and stimulated with plate-bound anti-CD3

331   (clone HIT3a) at 1ug/ml and soluble anti-CD28 (CD28.2) at 2ug/ml, or cells were activated with IL12 and

332   IL18 (PeproTech) at 50ng/mL for 12hours at 37°C in 4% $O_2$, and Brefeldin A was added for the last 4 hours.

333   After stimulation, cells were stained for intracellular cytokine production as described above. For the

334   inhibition assays, LP T cells were first incubated with anti-CD161-Biotin mAb (HP3G10, Biolegend or 191B8,

335   Miltenyi Biotec) and isotype controls IgG1 (MPOC-21, BioLegend) and IgG2a (MPOC-173, BioLegend) for

336   15 minutes, washed, and cross-linked with anti-Biotin Cocktail (STEMCELL Technologies) during stimulation

337   with anti-CD3/anti-CD28 or cytokines as described above.

338

339   **T cell isolation and RNA extraction for RNA sequencing.** PLZF$^+$ and PLZF$^-$ CD4$^+$ TCRβ$^+$ T cells were

340   sorted using a FACS Aria2 SORP (BD Biosciences). T cells were isolated as described above from the

341   intestine of 5 individual samples, and MAIT cells were pooled from the intestine and MLN for RNA

342   sequencing (RNAseq) as outlined in Extended Fig. 2a and $10^4$ cells were collected per subset for each

343    sample. Post-sort purity was determined by flow cytometry following intracellular staining for PLZF as above

344    and was >92% for PLZF⁻ T cells and MAIT cells, and >87% for PLZF⁺ T cells.  RNA was extracted and

345    purified with the Dynabeads mRNA DIRECT Purification Kit (Thermo Fisher Scientific). mRNA libraries were

346    constructed using the Nugen/Nextera XT Library Prep Kit (Illumina), and 15 samples (5 donors, 3 T cell

347    subsets) were sequenced on an Illumina HiSeq 4000 by the Functional Genomics Core Facility at the

348    University of California, San Francisco. The reads from the Illumina Hi-seq sequencer in fastq format were

349    verified for quality control using fastqc software package and reads were aligned to the Human genome

350    (hg38) and read counts aggregated by gene using the Ensembl GRCh38.78 annotation using STAR [49].

351    Differential gene expression analysis was performed with DESeq2 v1.16.1 package [50].

352    **Statistical analysis.** Groups were compared with Prism Version 5 software (GraphPad) using the Wilcoxon

353    matched-pairs signed rank test or the Kruskal Wallis with Dunn's Multiple comparison test. Box plot

354    rectangles show first to third quartile, the line shows the median and the whiskers represent minimum and

355    maximum values, unless otherwise stated. Correlation analysis was measured by Spearman correlation

356    coefficient. Bar plots represent the mean and the standard error of the mean. $p < 0.05$ was considered

357    significant. Principle component analysis and accompanying confidence intervals were performed using

358    combined functions in the R packages 'stats', 'vegan', and 'ggplot2', and PERMANOVA analysis was used

359    assess the significance of the Euclidean distances between the groups. Heatmaps were generated using the

360    R packages 'heatmap' and 'circlize'. A co-expression analysis was performed for the differentially expressed

361    (DE) genes using the Human Primary Cell Atlas [29]. This atlas contains 713 microarray samples of a wide

362    range of pure cell types and states. The complexity of the dataset was reduced to the median gene

363    expression per cell state (N=157), and Spearman correlation coefficients were calculated for each pair of DE

364    genes, revealing clusters of genes that are co-expressed in the same set of cell types.  Gene clusters were

365    analyzed for overlap with KEGG and GO biological processes gene sets using the Molecular Signatures

366    Database (MSigDB) [51,52]. No statistical methods were used to predetermine sample size. The experiments

367    were not randomized and the investigators were not blinded to allocation during experiments and outcome

368    assessment.

369

370    **Data and software availability.** RNA-Seq data that support the findings of this study have been deposited

371    in NCBI BioProject with the primary accession code PRJNA438160.

372    (http://www.ncbi.nlm.nih.gov/bioproject/438160). Further data that support the findings of this study are

373    available from the corresponding authors upon request.

374

**Acknowledgements**

**Author contributions**

JH conceived of and designed the study, performed research, analyzed the data, and wrote the manuscript; ER contributed to study design, performed research, and manuscript development; DA contributed to bioinformatics analysis and created figures for manuscript; VM performed immune cell isolations; WE contributed to data analysis; TDB contributed to study design. All authors discussed the results and edited the manuscript.

Competing Financial interests

The authors have no competing interests to disclose.

Correspondence and requests for materials should be addressed to Joanna.Halkias@ucsf.edu.

**REFERENCES**

402   1.   Orlic, D. & Lev, R. An electron microscopic study of intraepithelial lymphocytes in human
403        fetal small intestine. *Lab. Invest.* **37,** 554–561 (1977).
404   2.   Spencer, J., Dillon, S. B., Isaacson, P. G. & MacDonald, T. T. T cell subclasses in fetal
405        human ileum. *Clin. Exp. Immunol.* **65,** 553–558 (1986).
406   3.   Mold, J. E. *et al.* Maternal alloantigens promote the development of tolerogenic fetal
407        regulatory T cells in utero. *Science (New York, N.Y.)* **322,** 1562–1565 (2008).
408   4.   Hermann, E. *et al.* Human fetuses are able to mount an adultlike CD8 T-cell response.
409        *Blood* **100,** 2153–2158 (2002).
410   5.   Malhotra, I. *et al.* In utero exposure to helminth and mycobacterial antigens generates
411        cytokine responses similar to that observed in adults. *J. Clin. Invest.* **99,** 1759–1766
412        (1997).
413   6.   Marchant, A. *et al.* Mature CD8+ T lymphocyte response to viral infection during fetal life.
414        *J. Clin. Invest.* **111,** 1747–1755 (2003).
415   7.   Gomez, R. *et al.* The fetal inflammatory response syndrome. *American Journal of
416        Obstetrics and Gynecology* **179,** 194–202 (1998).
417   8.   Romero *et al.* A fetal systemic inflammatory response is followed by the spontaneous
418        onset of preterm parturition. *American Journal of Obstetrics and Gynecology* **179,** 8–8
419        (1998).
420   9.   Crespo, M. *et al.* Neonatal T-cell maturation and homing receptor responses to Toll-like
421        receptor ligands differ from those of adult naive T cells: relationship to prematurity. *Pediatr
422        Res* **71,** 136–143 (2011).
423   10.  Duggan, P. J. *et al.* Intrauterine T-cell activation and increased proinflammatory cytokine
424        concentrations in preterm infants with cerebral lesions. *The Lancet* **358,** 1699–1700
425        (2001).
426   11.  Luciano, A. A., Yu, H., Jackson, L. W., Wolfe, L. A. & Bernstein, H. B. Preterm Labor and
427        Chorioamnionitis Are Associated with Neonatal T Cell Activation. *PLoS ONE* **6,** e16698
428        (2011).
429   12.  Bunders, M. J. *et al.* Memory CD4+CCR5+ T cells are abundantly present in the gut of
430        newborn infants to facilitate mother-to-child transmission of HIV-1. *Blood* **120,** 4383–4390
431        (2012).
432   13.  Thome, J. J. C. *et al.* Early-life compartmentalization of human T cell differentiation and
433        regulatory function in mucosal and lymphoid tissues. *Nat. Med.* **22,** 72–77 (2016).
434   14.  Zhang, X. *et al.* CD4 T cells with effector memory phenotype and function develop in the
435        sterile environment of the fetus. *Science Translational Medicine* **6,** 238ra72–238ra72
436        (2014).
437   15.  Muench, M. O., Bärtsch, E. M. P., Chen, J.-C., Lopoo, J. B. & Bárcena, A. Ontogenic
438        changes in CD95 expression on human leukocytes: prevalence of T-cells expressing
439        activation markers and identification of CD95−CD45RO+ T-cells in the fetus.
440        *Developmental & Comparative Immunology* **27,** 899–914 (2003).
441   16.  Sathaliyawala, T. *et al.* Distribution and Compartmentalization of Human Circulating and
442        Tissue-Resident Memory T Cell Subsets. *Immunity* **38,** 187–197 (2013).
443   17.  Thome, J. J. C. *et al.* Spatial Map of Human T Cell Compartmentalization and
444        Maintenance over Decades of Life. *Cell* **159,** 814–828 (2014).
445   18.  Spencer, J., MacDonald, T. T., Finn, T. & Isaacson, P. G. The development of gut
446        associated lymphoid tissue in the terminal ileum of fetal human intestine. *Clin. Exp.
447        Immunol.* **64,** 536–543 (1986).
448   19.  Mueller, S. N. & Mackay, L. K. Tissue-resident memory T cells: local specialists in immune
449        defence. *Nature Rev. Immunol.* **16,** 79–89 (2015).
450   20.  Lee, Y. J. *et al.* Generation of PLZF+ CD4+ T cells via MHC class II-dependent
451        thymocyte-thymocyte interaction is a physiological process in humans. *Journal of
452        Experimental Medicine* **207,** 237–246 (2010).
453   21.  Fergusson, J. R. *et al.* CD161 Defines a Transcriptional and Functional Phenotype across
454        Distinct Human T Cell Lineages. *CellReports* **9,** 1075–1088 (2014).
455   22.  Halkias, J. *et al.* Conserved and divergent aspects of human T-cell development and
456        migration in humanized mice. *Immunology and Cell Biology* **93,** 716–726 (2015).

23. Howie, D. *et al.* Extrathymic T cell differentiation in the human intestine early in life. *J. Immunol.* **161,** 5862–5872 (1998).

24. Loh, L., Ivarsson, M. A., Isson, J. M. E., Sandberg, J. K. & Nixon, D. F. Invariant natural killer T cells developing in the human fetus accumulate and mature in the small intestine. *Mucosal Immunology* **7,** 1233–1243 (2014).

25. Kumar, B. V. *et al.* Human Tissue-Resident Memory T Cells Are Defined by Core Transcriptional and Functional Signatures in Lymphoid and Mucosal Sites. *CellReports* **20,** 2921–2934 (2017).

26. Reantragoon, R. *et al.* Antigen-loaded MR1 tetramers define T cell receptor heterogeneity in mucosal-associated invariant T cells. *Journal of Experimental Medicine* **210,** 2305–2320 (2013).

27. Leeansyah, E., Loh, L., Nixon, D. F. & Sandberg, J. K. Acquisition of innate-like microbial reactivity in mucosal tissues during human fetal MAIT-cell development. *Nature Communications* **5,** 3143 (2014).

28. Ben Youssef, G. *et al.* Ontogeny of human mucosal-associated invariant T cells and related T cell subsets. *Journal of Experimental Medicine* **215,** 459–479 (2018).

29. Mabbott, N. A., Baillie, J. K., Brown, H., Freeman, T. C. & Hume, D. A. An expression atlas of human primary cells: inference of gene function from coexpression networks. *BMC Genomics* **14,** 632 (2013).

30. Gold, M. C. *et al.* MR1-restricted MAIT cells display ligand discrimination and pathogen selectivity through distinct T cell receptor usage. *Journal of Experimental Medicine* **211,** 1601–1610 (2014).

31. Howson, L. J. *et al.* MAIT cell clonal expansion and TCR repertoire shaping in human volunteers challenged with Salmonella Paratyphi A. *Nature Communications* **9,** 1–11 (2018).

32. Rechavi, E. *et al.* Timely and spatially regulated maturation of B and T cell repertoire during human fetal development. *Science Translational Medicine* **7,** 276ra25–276ra25 (2015).

33. Le Bourhis, L. *et al.* MAIT Cells Detect and Efficiently Lyse Bacterially-Infected Epithelial Cells. *PLoS pathogens* **9,** e1003681–12 (2013).

34. Rosen, D. B. *et al.* Cutting edge: lectin-like transcript-1 is a ligand for the inhibitory human NKR-P1A receptor. *J. Immunol.* **175,** 7796–7799 (2005).

35. Kamada, N. *et al.* Human CD14+ Macrophages in Intestinal Lamina Propria Exhibit Potent Antigen-Presenting Ability. *J. Immunol.* **183,** 1724–1731 (2009).

36. Bain, C. C. *et al.* Resident and pro-inflammatory macrophages in the colon represent alternative context-dependent fates of the same Ly6Chi monocyte precursors. *Mucosal Immunology* **6,** 498–510 (2012).

37. Ikuta, K. *et al.* A developmental switch in thymic lymphocyte maturation potential occurs at the level of hematopoietic stem cells. *Cell* **62,** 863–874 (1990).

38. Hardy, R. R. & Hayakawa, K. A developmental switch in B lymphopoiesis. *Proc. Natl. Acad. Sci. U.S.A.* **88,** 11550–11554 (1991).

39. Dimova, T. *et al.* Effector Vγ9Vδ2 T cells dominate the human fetal γδ T-cell repertoire. *Proceedings of the National Academy of Sciences* **112,** E556–65 (2015).

40. de Lalla, C. *et al.* High-frequency and adaptive-like dynamics of human CD1 self-reactive T cells. *Eur. J. Immunol.* **41,** 602–610 (2011).

41. Dong, M. *et al.* Alterations in the Thymic Selection Threshold Skew the Self-Reactivity of the TCR Repertoire in Neonates. *J. Immunol.* **199,** 965–973 (2017).

42. Michaëlsson, J., mold, J. E., McCune, J. M. & Nixon, D. F. Regulation of T cell responses in the developing human fetus. *J. Immunol.* **176,** 5741–5748 (2006).

43. Aagaard, K. *et al.* The Placenta Harbors a Unique Microbiome. *Science Translational Medicine* **6,** 237ra65–237ra65 (2014).

44. Ardissone, A. N. *et al.* Meconium Microbiome Analysis Identifies Bacteria Correlated with Premature Birth. *PLoS ONE* **9,** e90784 (2014).

45. Collado, M. C., Rautava, S., Aakko, J., Isolauri, E. & Salminen, S. Human gut colonisation may be initiated in utero by distinct microbial communities in the placenta and amniotic fluid. *Scientific Reports* **6,** 1–13 (2016).

513   46.   Elahi, S. *et al.* Immunosuppressive CD71+ erythroid cells compromise neonatal host
514         defence against infection. *Nature* **504,** 158–162 (2013).
515   47.   McGovern, N. *et al.* Human fetal dendritic cells promote prenatal T-cell immune
516         suppression through arginase-2. *Nature* **546,** 1–19 (2017).
517   48.   Zhivaki, D. *et al.* Respiratory Syncytial Virus Infects Regulatory B Cells in Human
518         Neonates via Chemokine Receptor CX3CR1 and Promotes Lung Disease Severity.
519         *Immunity* **46,** 301–314 (2017).
520   49.   Dobin, A. *et al.* STAR: ultrafast universal RNA-seq aligner. *Bioinformatics (Oxford,*
521         *England)* **29,** 15–21 (2013).
522   50.   Anders, S. & Huber, W. Differential expression analysis for sequence count data. *Genome*
523         *Biol.* **11,** R106 (2010).
524   51.   Subramanian, A. *et al.* Gene set enrichment analysis: a knowledge-based approach for
525         interpreting genome-wide expression profiles. *Proc. Natl. Acad. Sci. U.S.A.* **102,** 15545–
526         15550 (2005).
527   52.   Liberzon, A. *et al.* Molecular signatures database (MSigDB) 3.0. *Bioinformatics* **27,** 1739–
528         1740 (2011).
529
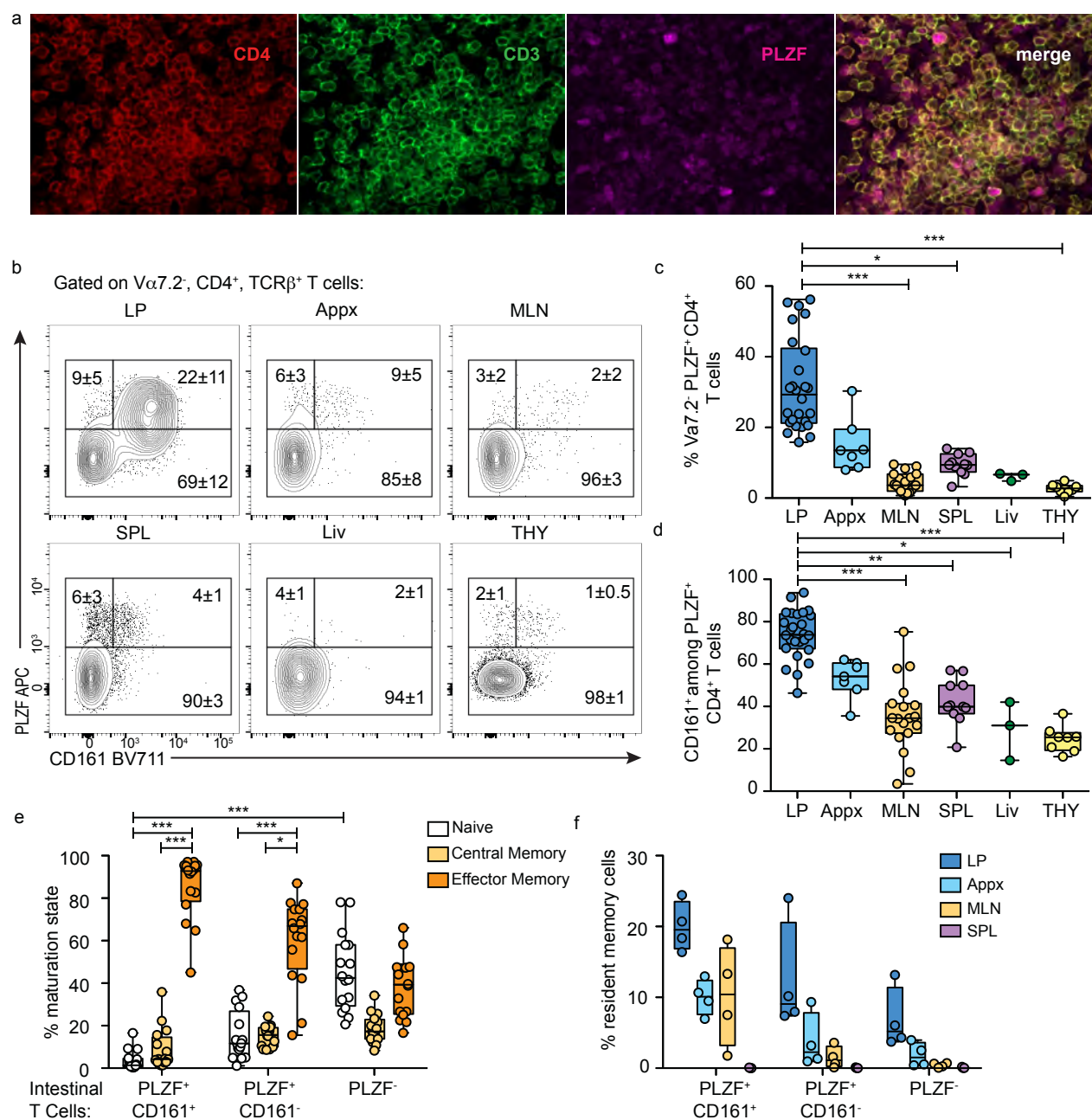
Figure 1



**Figure 1: The fetal small intestine is enriched for PLZF+ CD4+ T cells**

a, Representative imaging (40x) of PLZF expression in the lamina propria of the small intestine (n=3). b, Representative flow plots of PLZF and CD161 expression among CD4+ T cells in fetal tissues. c, Frequencies of PLZF+ CD4+ T cells and d, Proportion of CD161+ cells among PLZF+ CD4+ T cells in fetal tissues. e, Frequencies of Naïve (CD45RA+, CCR7+), Central Memory (CD45RA-, CCR7+), and Effector Memory (CD45RA-, CCR7-) phenotypes within indicated populations of intestinal CD4+ T cells. f, Frequencies of resident memory populations within indicated subsets of CD4+ T cells. Circles represent individual donors (c-d, e-f). Significance was measured by Kruskal Wallis paired ANOVA with Dunn's multiple comparison test (c-d, e-f). *p < 0.05, **p < 0.005, ***p < 0.0005. Numbers in the flow cytometry plots correspond to the frequencies of gated populations ± SD.

Figure 2
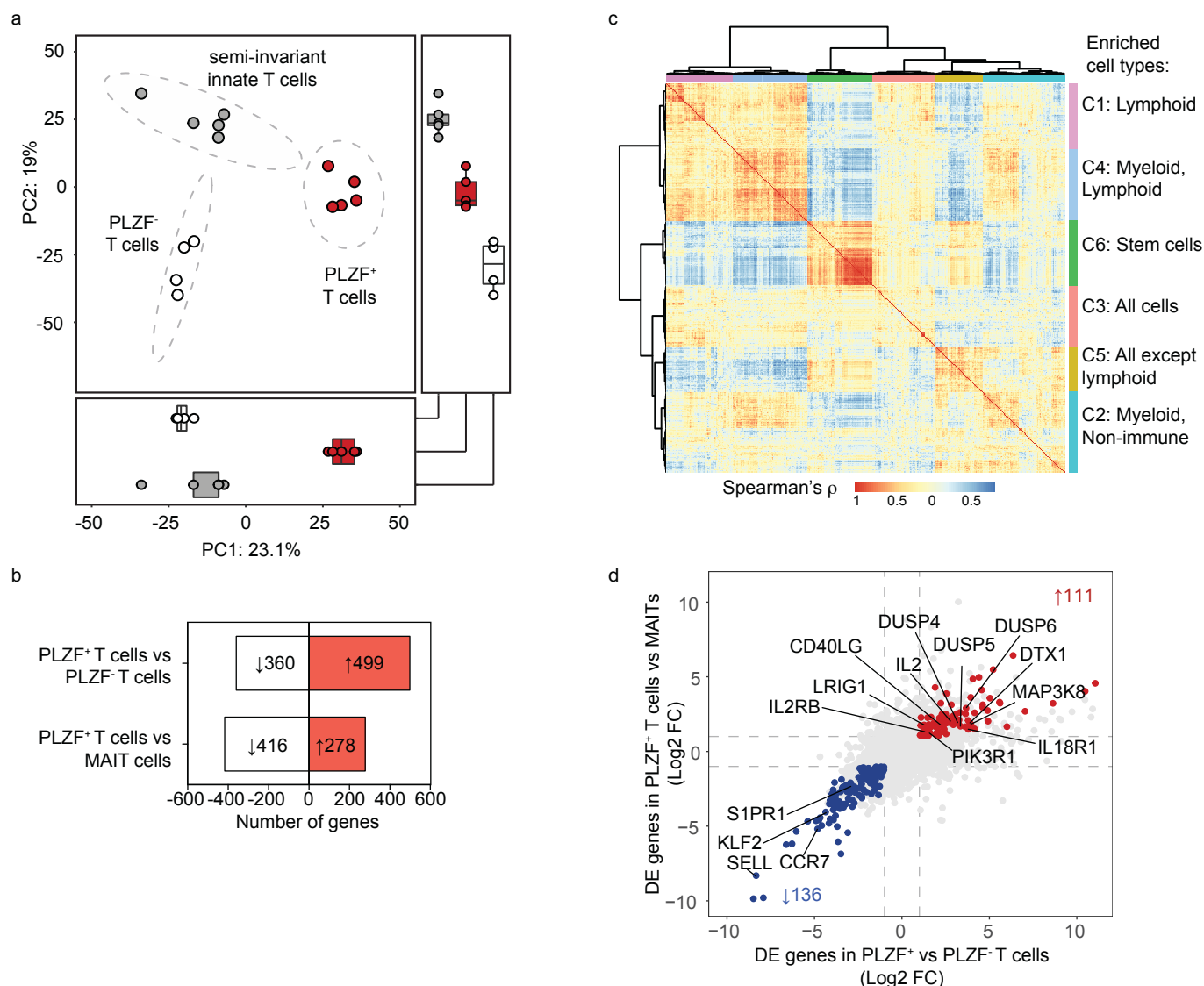


**Figure 2: PLZF+ CD161+ CD4+ T cells are a distinct population of fetal T cells**

a, Principal component analysis (PCA) of the top 1000 variable genes identified by RNAseq of fetal intestinal PLZF+ T cells (n=5), PLZF- T cells (n=4), and semi-invariant innate T cells cells n=5). Ellipses denote the 95% confidence intervals of the population means (PERMANOVA R2 0.92, p<0.001). Boxplots indicate scores for PC1 (bottom), and PC2 (right). b, Numbers of genes with >2 fold (FDR<0.05) increase (red) or decrease (white) in expression levels between the indicated populations. c, Correlation analysis using the Human Primary Cell Atlas as a reference of the differentially expressed genes (>2 fold, FDR<0.05) in PLZF+ T cells as compared to PLZF- T cells revealing clusters of genes (C1-C6) that are co-expressed in the same cell types. d, Multi-way comparison of differentially expressed genes (>2 fold, FDR<0.05) in PLZF+ T cells compared to MAIT cells (y-axis) and compared to PLZF- T cells (x-axis) identifies a core signature of genes uniquely enriched (red) and uniquely depleted (blue) within PLZF+ T cells. Selected genes involved in immune response, immune regulation, and leukocyte migration are labeled.
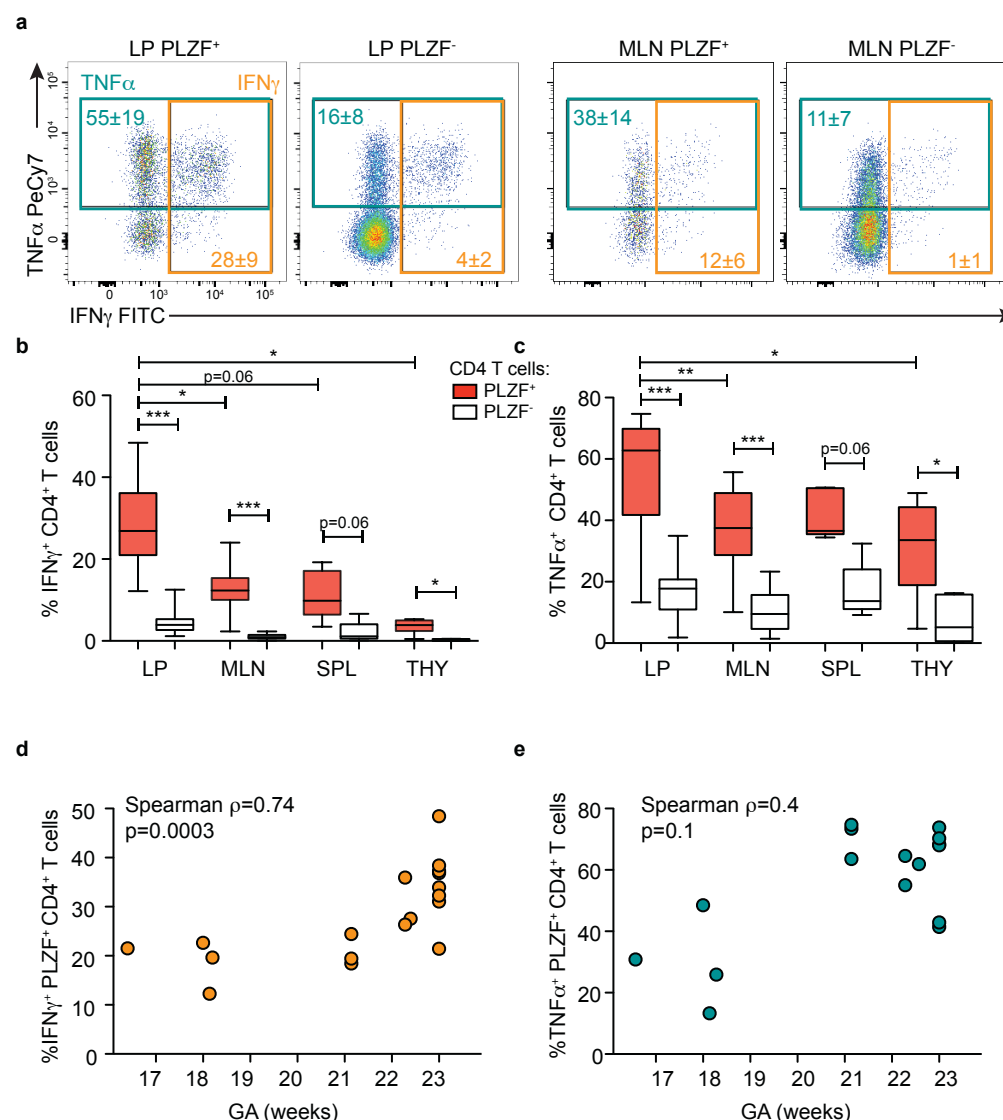
Figure 3



**Figure 3: PLZF+ CD4 T cells possess a distinct functional signature**
a, Representative flow plots of intracellular TNFα and IFNγ staining of indicated populations of intestinal, MLN, and adult PB live Vα7.2-TCRβ+CD4+T cells after PMA/Ionomycin stimulation. Numbers represent mean ± SD of gated frequencies. (n=18). Frequencies of b, IFNγ+ and c, TNFα+ cells within indicated populations of Vα7.2-TCRβ+CD4+T cells after PMA/Ionomycin stimulation within fetal LP (n=18), MLN (n=11), SPL (n=5), and THY (n=6). d, e, Spearman's rank correlation was used to calculate the association between d, IFNγ and e, TNFα production by intestinal PLZF+ CD4 T cells in response to PMA/Ionomycin and weeks of gestational age (GA). Circles represent individual donors. Wilcoxon matched-pairs signed rank test (b, c). *p < 0.05, ***p < 0.001.

Figure 4
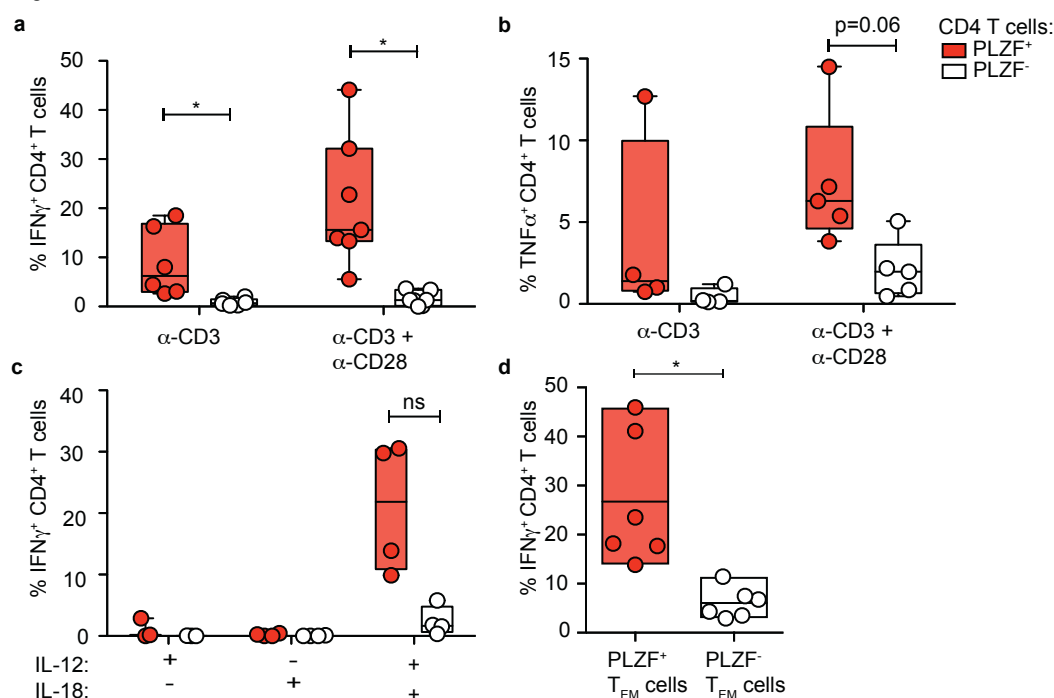


**Figure 4: Dual activation of PLZF+ T cells**

a, b Frequencies of a, IFNγ+ and b, TNFα+ cells within indicated populations of intestinal live Vα7.2-TCRβ+CD4+T cells after 12-14hrs of TCR stimulation with anti-CD3 +/- anti-CD28. c, Frequencies of IFNγ+ cells within indicated populations of intestinal Vα7.2-TCRβ+CD4+T cells after 12-14hrs of cytokine stimulation with IL-12 and/or IL-18. d, Frequencies of IFNγ+ cells among intestinal PLZF+ and PLZF- TEM cells in response to TCR stimulation with anti-CD3 + anti-CD28. Floating bars span minimum and maximum, line represents mean. Circles represent individual donors. Wilcoxon matched-pairs signed rank test (a-d), *p < 0.05, ns= not significant.
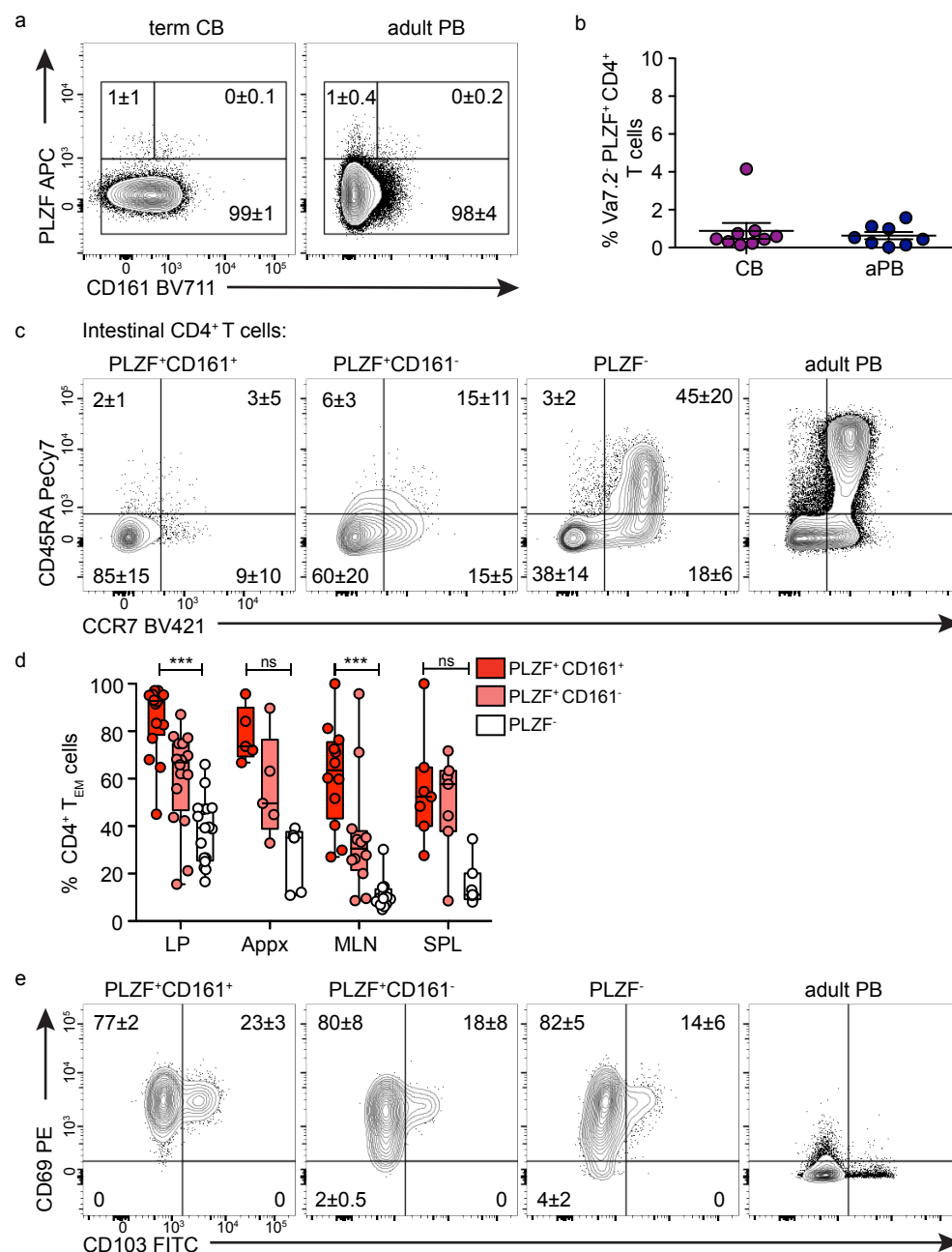
Figure 5
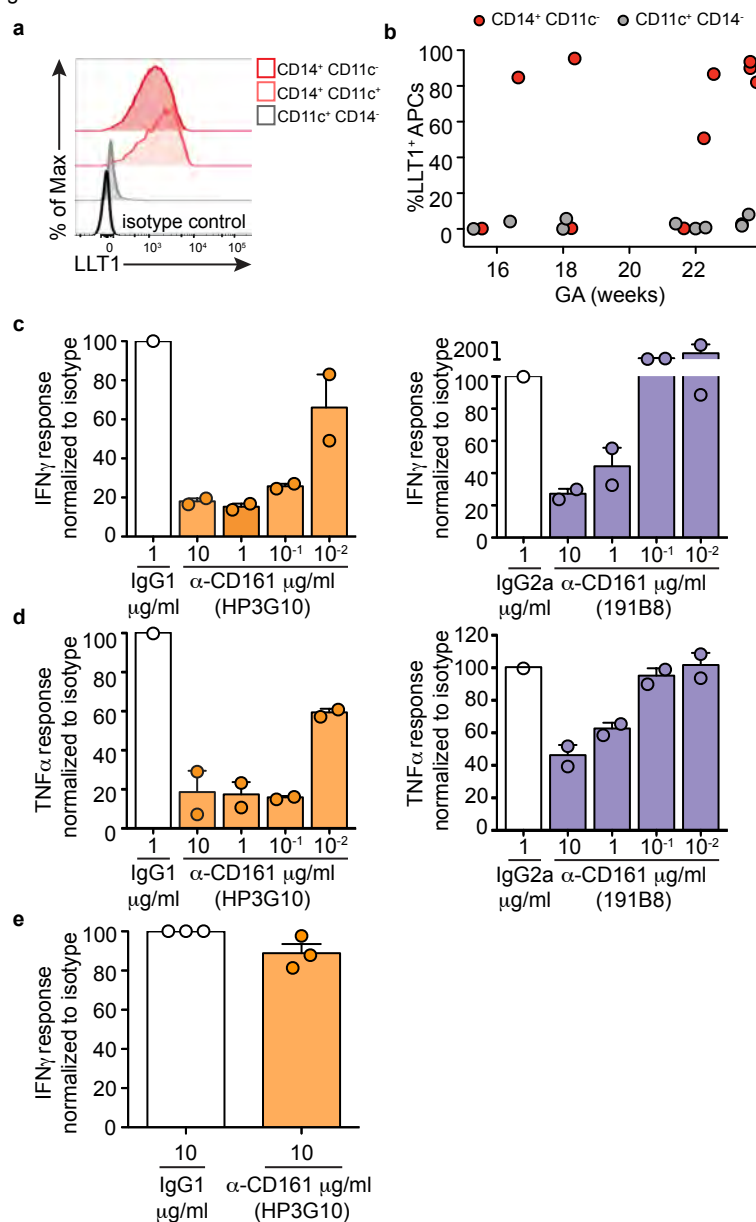


**Figure 5: CD161 inhibits production of IFNγ in PLZF+ T cells**
a, Histogram of LLT1 expression on indicated intestinal APC subsets. b, Summary of frequencies of LLT1 expression among dendritic cells (CD11c+ CD14-, grey) and macrophages (CD14+ CD11c-, red) of the fetal small intestine relative to gestational age (GA) in weeks. Circles represent individual samples. c, d, Relative proportions of c, IFNγ+ and d, TNFα+ PLZF+ Vα7.2-TCRβ+CD4+T cells after 12-14hrs stimulation with anti-CD3/anti-CD28 in the presence of biotinylated isotypes or anti-CD161 antibodies ligated with anti-biotin beads. One representative experiment of 4 is shown. Bar represents mean with SEM, circles represent technical replicates.  e, Relative proportions of IFNγ+ PLZF+ Vα7.2-TCRβ+CD4+T cells after 12-14hrs stimulation with IL-12+IL18 in the presence of biotinylated isotype or anti-CD161 antibodies ligated with anti-biotin beads. Circles represent individual donors. Proportions of IFNγ+ and TNFα+ cells are normalized to isotype response. Two different anti-CD161 clones are shown (HP3G10 in orange and 191B8 in purple).
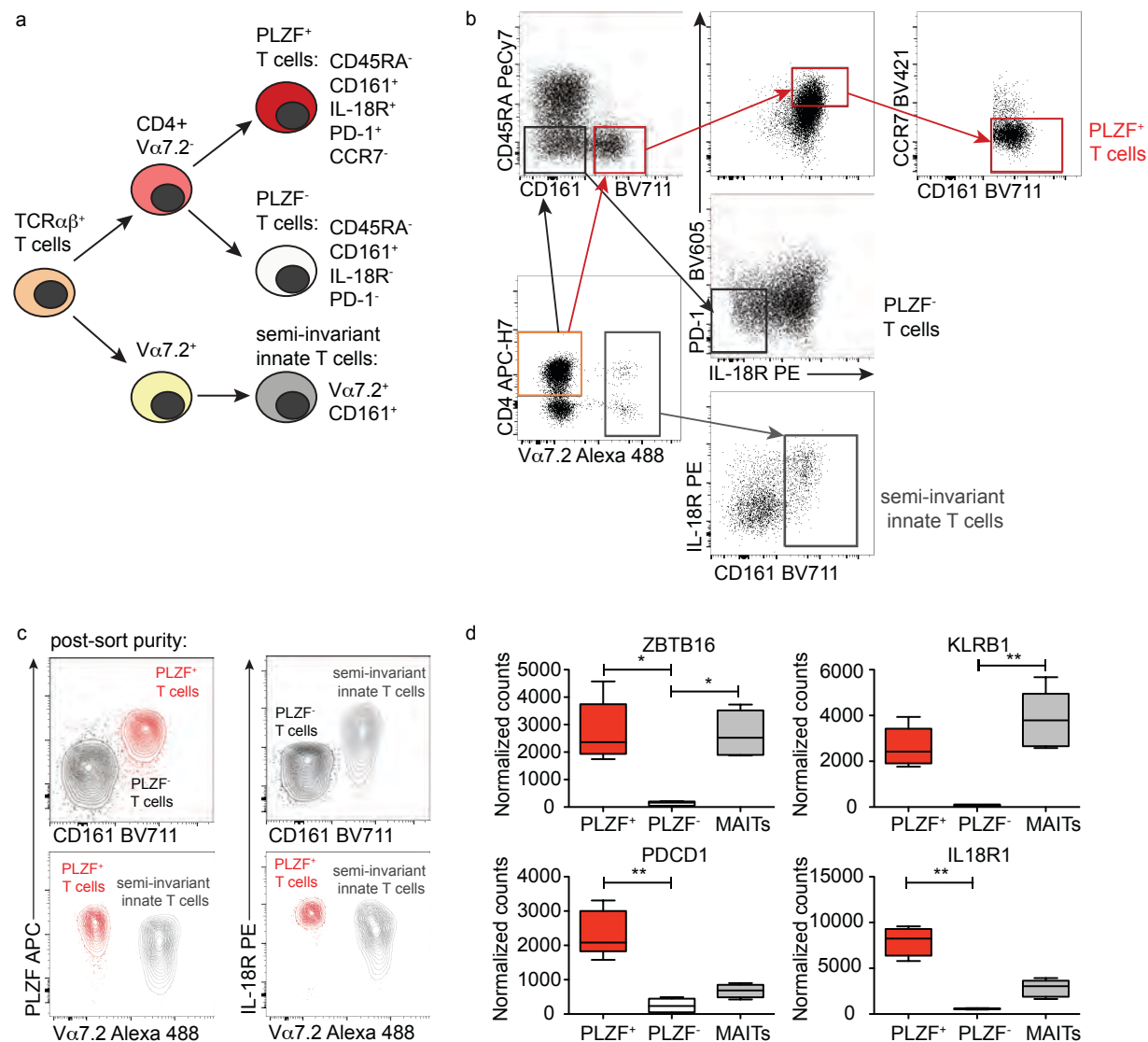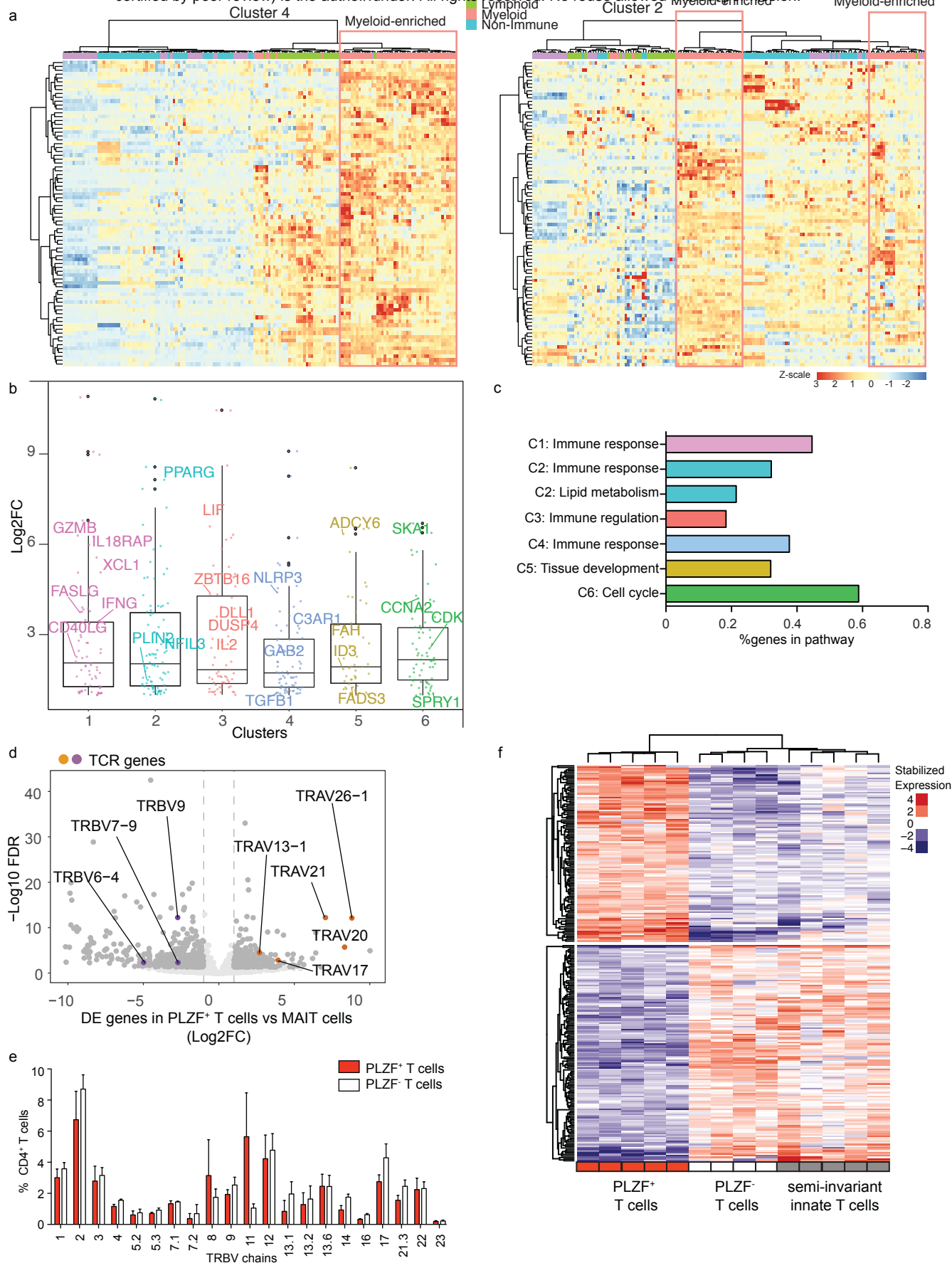
Extended Figure 1



**Extended Figure 1: PLZF+ CD4+ T cells are enriched in the fetal small intestine and possess a resident memory phenotype**

All samples gated on Vα7.2-TCRβ+CD4+T cells. a, Representative flow plots of PLZF and CD161 expression among CD4+ T cells in term cord blood (CB) and adult peripheral blood (PB). b, Frequencies of PLZF+ CD4+ T cells in term cord blood (CB) and adult peripheral blood (PB). Line represents mean, error bars SEM. c, Representative flow plots of CD45RA and CCR7 expression among indicated subsets of intestinal CD4+ T cells and adult PB gating control. d, Frequencies of CD45RA- CCR7- TEM cells among indicated T cell subsets in fetal tissues. e, Proportions of Naïve, TCM, and TEM within indicated intestinal subsets of CD4+ T cells.e, Representative flow plots of CD69 and CD103 expression among indicated subsets of intestinal CD4+ TEM cells and adult PB gating control. Circles represent individual donors (d). Numbers in the flow cytometry plots correspond to the mean ± SD of gated populations.

**Extended Figure 2: Characteristics of sorted fetal T cell populations**
a, Schematic representation of strategy for the identification and isolation of indicated T cell populations.  b, Gating strategy for PLZF+ T cells, PLZF- T cells, and MAIT cells after sorting on live, TCRβ+ intestinal T cells. c, Representative flow plots of post-sort purity after intra-nuclear staining for PLZF. d, Boxplots show quantification of RNAseq normalized read counts of indicated genes among sorted populations. *p<0.05, **p<0.01.  Kruskal Wallis with Dunn's Multiple comparison test (d).

**Extended Figure 3: Distinct transcriptional signature of PLZF+ T cells**

a, Heatmap shows color-coded relative enrichment of differentially expressed genes in PLZF+ T cells relative to PLZF- T cells among indicated cell types identified from the Human Primary Cell Atlas for Cluster 4 (left) and Cluster 2 (right). b, Comparison of differentially expressed genes in PLZF+ T cells relative to PLZF- T cells identified in Figure 2c. Boxplots show median (centre line), interquartile range (box), 25- and 75 percentiles (whiskers), and outliers (dots above whiskers). c, Pathway analysis of gene clusters identified in Figure 2c was performed and gene pathways were organized into sub-clusters based on shared genes. Bar graphs show the % gene enrichment of each gene pathway within the indicated cluster. d, Volcano plot of differentially expressed genes (>2 fold, FDR<0.05) in PLZF+ T cells compared to MAIT cells. Differentially expressed genes are shown in dark grey, and TCR genes enriched (orange) or depleted (purple) in PLZF+ T cells are labeled. e, Relative levels of expression of 21 TCR Vβ chains on 3 separate intestinal samples. Levels of expression (mean ± SD) in PLZF+ CD4+ T cells (red) are compared to PLZF- CD4+ T cells (white). f, Hierarchical clustering of genes uniquely up- or down- regulated in PLZF+ T cells.
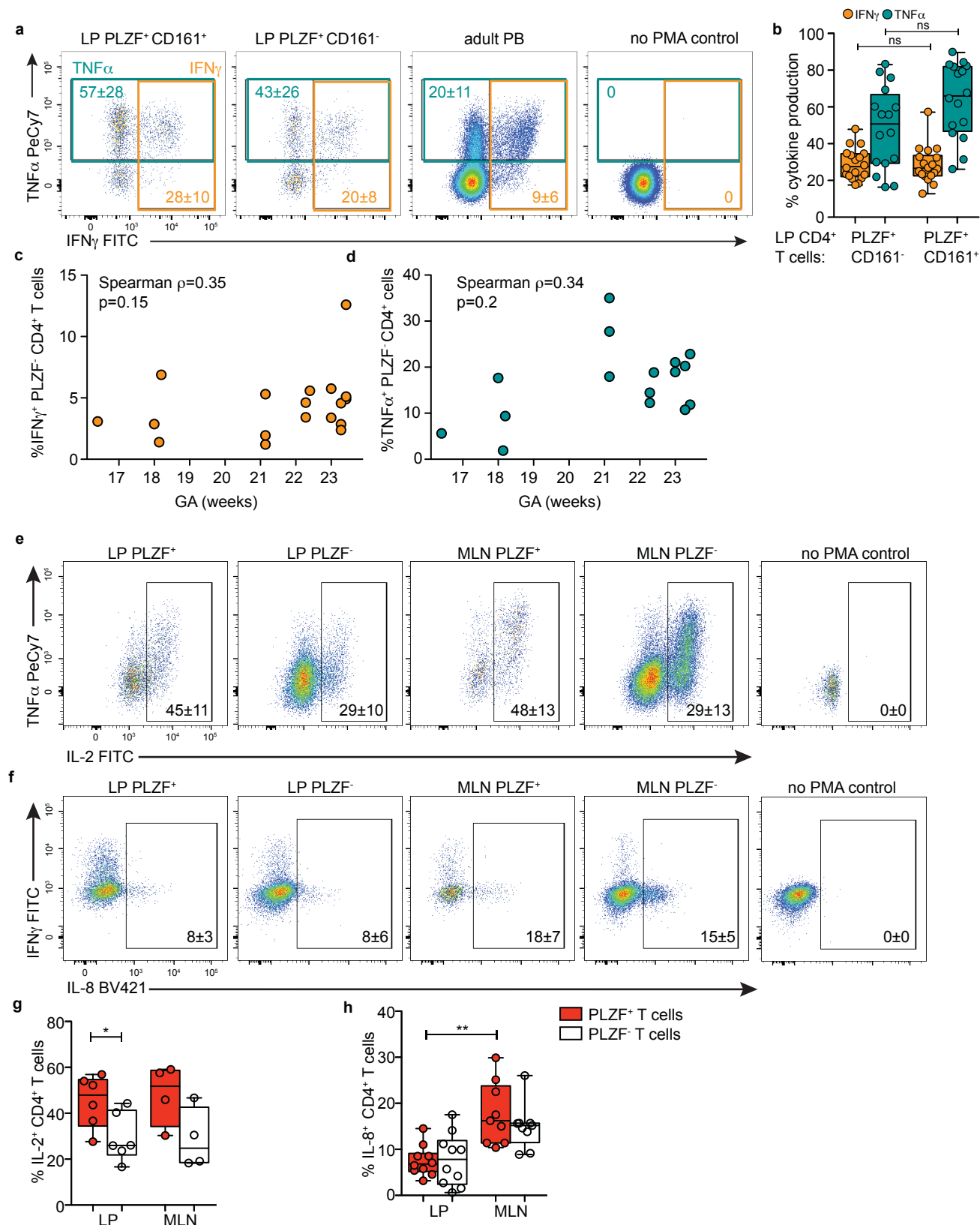
**Extended Figure 4: PLZF+ CD4 T cells are poised for rapid production of Th1 cytokines**

All samples gated on live Vα7.2-TCRβ+CD4+T cells. a, Representative flow plots of intracellular TNFα and IFNγ staining of indicated populations after PMA/Ionomycin stimulation of intestinal and adult PB CD4 T cells (n=18). b, Frequencies of IFNγ+ and TNFα+ cells within indicated populations of CD4 T cells after PMA/Ionomycin stimulation. c, d, Spearman's rank correlation was used to calculate the association between c, IFNγ and d, TNFα production by indicated subsets of intestinal CD4 T cells in response to PMA/Ionomycin. Circles represent individual donors. e-f, Representative flow plots of intracellular e, IL-2 and f, IL-8 after PMA/Ionomycin stimulation within indicated populations of intestinal and MLN CD4 T cells. g-h, Frequencies of g, IL-2+ and h, IL-8+ cells within indicated populations of CD4 T cells after PMA/Ionomycin stimulation within fetal LP and MLN. Numbers in the flow cytometry plots correspond to the mean ± SD of gated frequencies. Circles represent individual donors. Wilcoxon matched-pairs signed rank test (b, g, h). *p < 0.05, **p < 0.01.
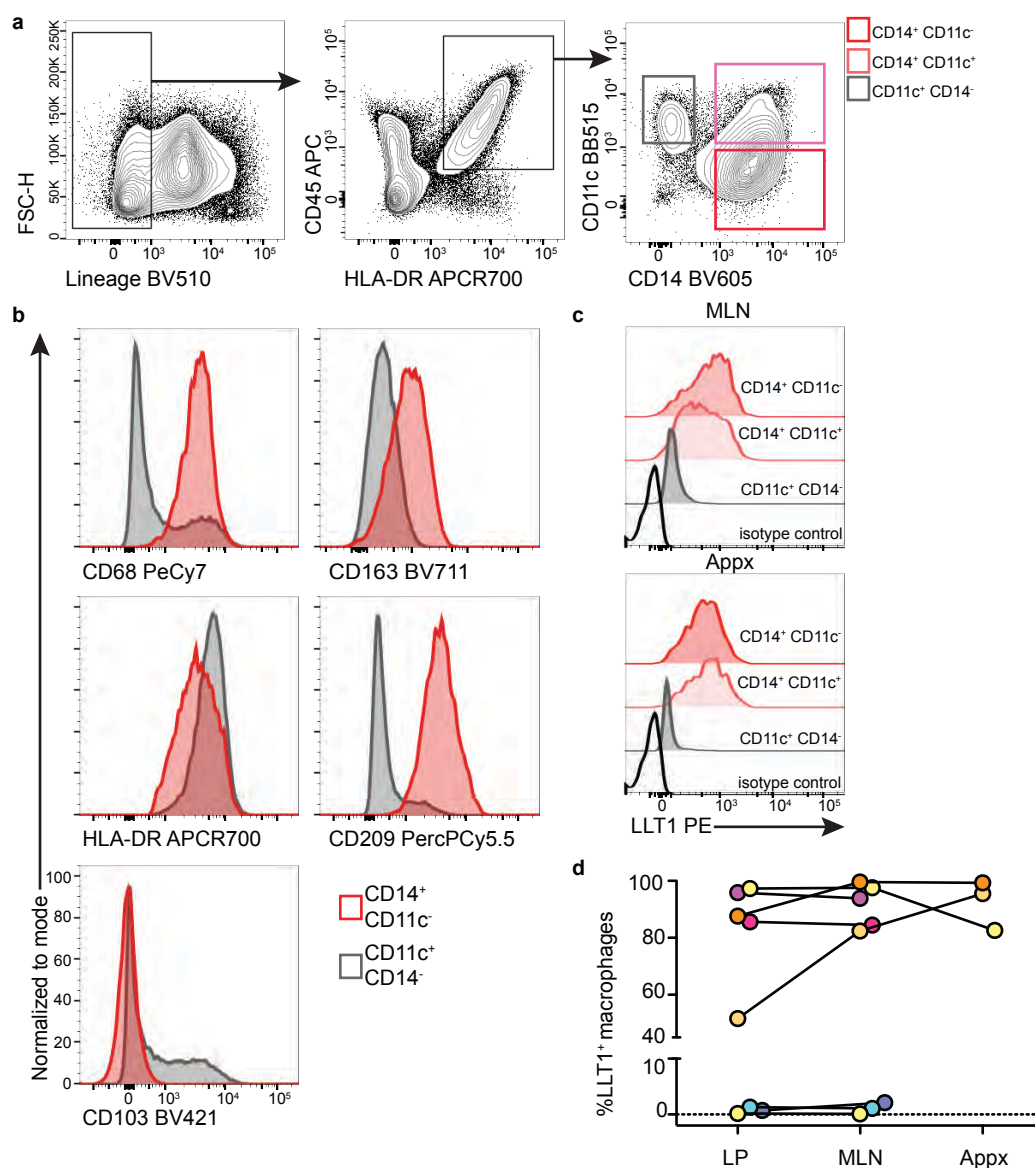
Extended Figure 5
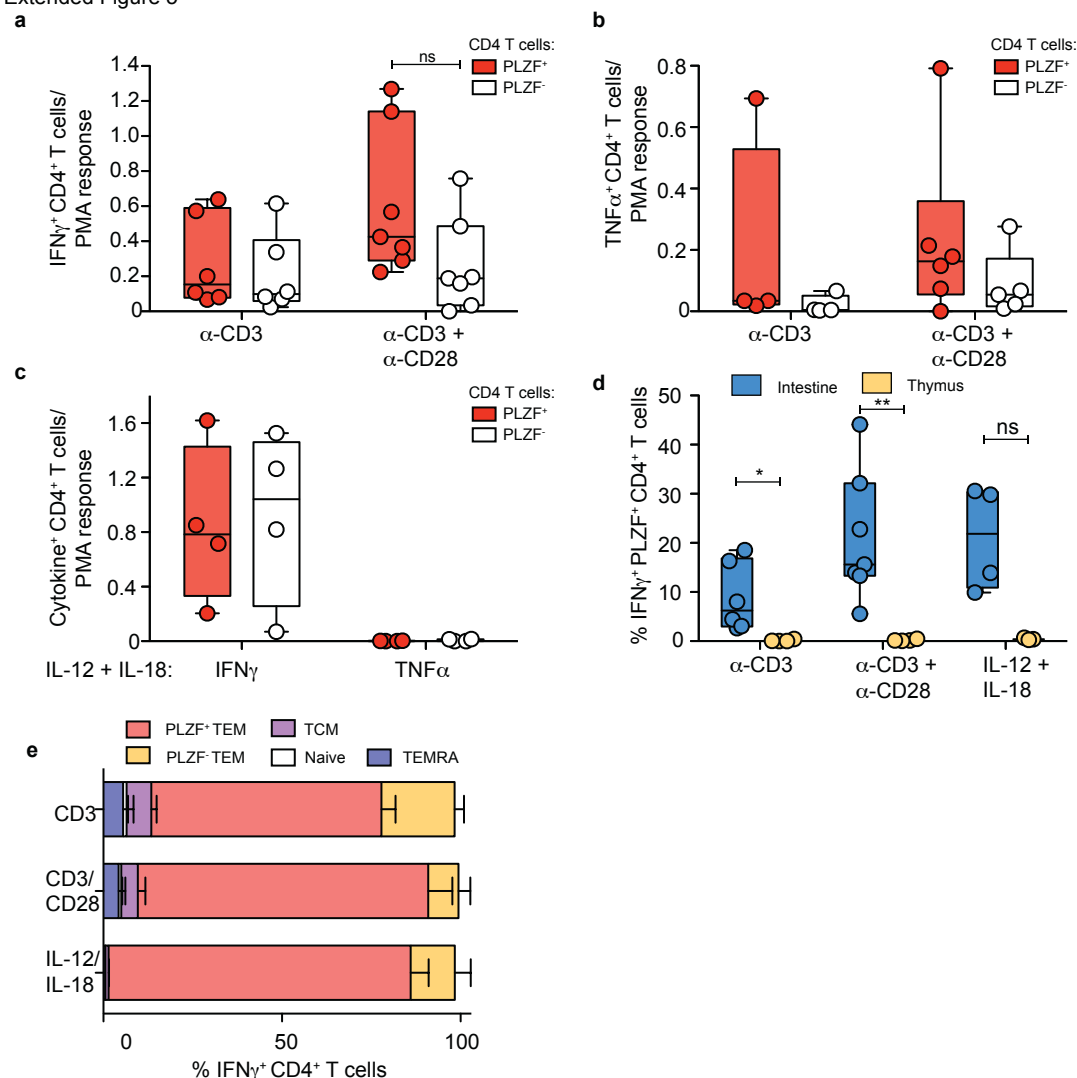


**Extended Figure 5: PLZF+ T cells produce Th1 cytokines in response to both TCR- and cytokine-mediated activation**

a, b Frequencies of a, IFNγ+ and b, TNFα+ cells relative to their PMA/Ionomycin potential within PLZF+ (red) and PLZF- (white) subsets of intestinal Vα7.2-TCRβ+CD4+T cells after 12-14hrs of TCR stimulation with anti-CD3 +/- CD28. c, Frequencies of IFNγ+ cells relative to their PMA/Ionomycin potential within PLZF+ (red) and PLZF- (white) subsets of intestinal Vα7.2-TCRβ+CD4+T cells after 12-14hrs of cytokine stimulation with IL-12 and/or IL-18. d, Comparison of intestinal and thymic frequencies of IFNγ+ PLZF+ Vα7.2-TCRβ+CD4+T cells after 12-14hrs of TCR- or cytokine-stimulation as indicated. e, Frequencies of memory and naïve cell subsets among intestinal IFNγ+ Vα7.2-TCRβ+CD4+T cells in response to 12-14hrs of TCR- (n=5) or cytokine-mediated (n=2) stimulation as indicated. Bar graphs denote mean +/- SEM (e). Circles represent individual donors (a-d, f). Wilcoxon matched-pairs signed rank test (a-d, e). *p < 0.05, **p < 0.01.

Extended Figure 6



**Extended Figure 6: Intestinal macrophages express LLT1, the ligand for CD161**
a, Gating strategy for identification of antigen presenting cells (APCs) in fetal tissues. Cells are gated on live, Lineage- (CD3-, CD19-, CD20-, CD56-) intestinal cells and identified as CD45+ HLA-DR+ cells. APCs subsets are defined as CD11c+ CD14-, CD14+ CD11c+, and CD14+ CD11c-. b, Representative histograms of surface markers in CD14+ CD11c- intestinal macrophages as compared to CD11c+ CD14- dendritic cells (n= 12). c, Representative histograms of LLT1 expression on indicated APC subsets in fetal MLN (n=8) and appendix (Appx) (n=3). d, Frequencies of LLT1 expression in tissue macrophages (CD14+ CD11c-) linked by donor. Each color represents an individual donor.